Density Functional Study on Ligand Binding of Izoniazid Target in *Mycobacterium tuberculosis*

Thesis submitted for the Degree of
"Magister Philosophiae"

Student:
Sergio Pantano

Supervisor
Dr. Paolo Carloni

October 1999

Contents:

Acknowledgements

I gratefully thank my supervisor, Dr Paolo Carloni, for the possibility he give my to study here.

To Frank who teach me the background of CPMD calculations

To all my friends and room mates of the first year of the Condensed Matter sector who teach me Italian (for free!)

To Lore, Leo and Stefano, with who I have discussed the subject of the thesis and an infinite quantity of other things (computers and vital space among them) and to Paul for his help.

And finally, but most important, to Claudia and Alejandro for been patient.

Chapter I

Introduction

Isonicotinic acid hydrazide (isoniazid, Inh) has been a first-line chemotherapeutic agent in treating *Mycobacterium tuberculosis* aggression[1,2] from the early fifty's. However Inh action mechanisms as well as mechanisms conferring the bacteria Inh resistance are rather complex and not completely understood. Inh is first activated by the KatG protein, a catalase-peroxidase dual function enzyme coded by the *kat*G gene[3-5] and an electron sink (hydrogen peroxide)[4-6]. Subsequently, Inh in it's activated form (either an anion or a radical) targets an enoyl-acyl carrier protein reductase (ACPR), the InhA enzyme coded by the *Inh*A gene[7].

Inh is covalently bound to the NADH cofactor within the InhA active site pocket (Fig. 1.1). InhA catalyzes the reduction of elongating fatty acids chains linked to the carrier protein. The reaction products are then converted to very long chain β-branched fatty acids (mycolic acids)[8], which are vital for cell wall synthesis. Therefore, InhA inhibition may lead to an increased vulnerability to external oxidative attacks and eventually to bacterial death.

NADH + R–CH=CH–CO–S–ACP

INH

H₂O₂

DRUG ACTIVATION

KatG

InhA

ENZYME INHIBITION

INH+

NAD + R–CH₂–CH₂–CO–S–ACP

INHIBITION OF MYCOLIC ACIDS SYNTHESIS
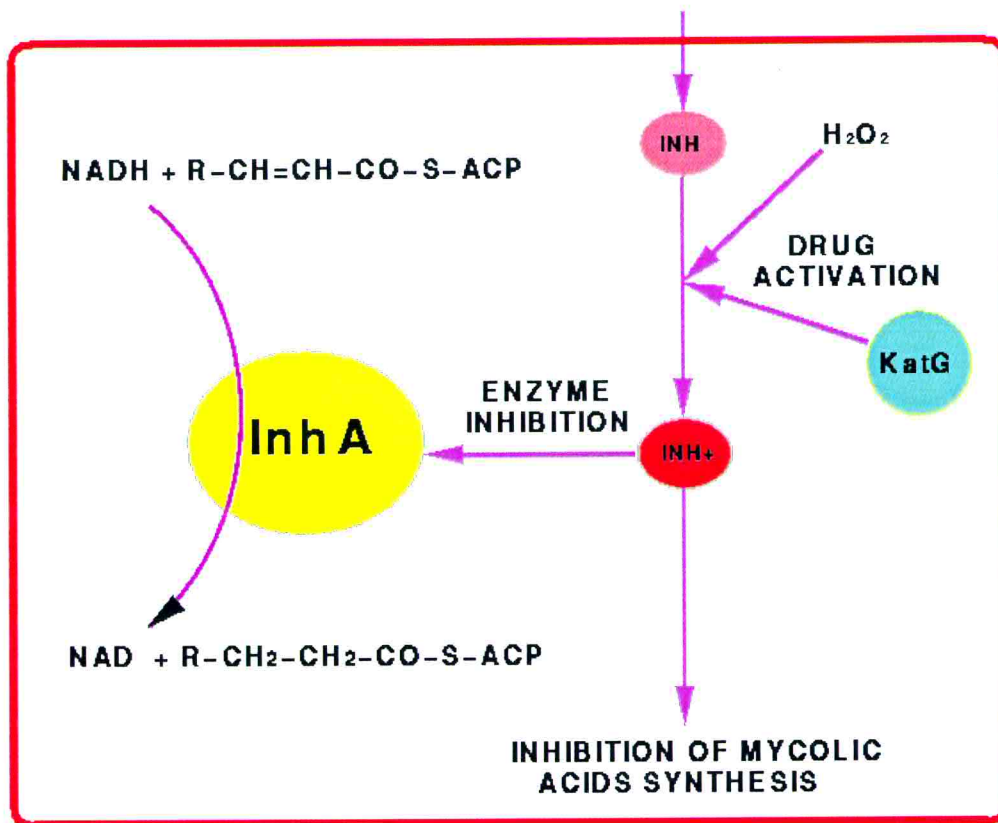
Drug benefit, however, is severely limited by the emergence of resistance, that is mutations introduced in the primary sequences of the enzymes that confer them the ability to overcome the drug action while retaining its biological function. It has been shown for InhA that resistance can be caused by single mutations either in the *InhA* or *katG* genes[9;10][11]. Those mutations are mainly due to a small degree of randomness in the replication process. Mutant strains emerge the in presence of antibacterial agents only when the balance of mutant reproduction is favorable, namely, mutations offer the bacteria a selective advantage against drug effect.

In Mycobacterium Tuberculosis, drug resistance commonly arises due to patient non compliance, or improper diagnosis. The new incidence of incurable cases and multi drug resistance strains, which are on the rise, has renewed the interest in clarifying the basis of the molecular mechanisms of the action of this and other antitubercular drugs.

Figure 1.1: Chemical structure of WT Inh-NADH complex. Inh and side chain of S94 are colored in red and pink, respectively. Protein residues are black, NADH is green. H-bond pattern is indicated in blue dashed lines. Figure adapted from Ref. 5.

Recent crystallographic studies by Sacchettini et al.[5;12;13 12;13] have offered the opportunity to analyze the structural changes associated with the InhA enzyme point mutation of Serine by Alanine at position 94 (S94A) that has been proposed to be involved in drug resistance. The X-ray crystal structures of both wild type (WT) and S94A InhA / Inh-NADH complexes have been determined at 2.1 and 2.7 Å resolution[12] respectively.

The H-bond network at the Inh-NADH binding site is shown in Fig.1.1. In WT InhA, Ser94 forms a water-mediated H-bond interaction with the β-phosphate moiety of the cofactor. This interaction is rather weak $(d(O\gamma_{(S94)}-Ow)=3.1$ Å, $d(Ow-O2)=3.3$ Å and is lost in the S94A mutant.

With the aim of shed light on the structural, dynamical and electronic structural aspects of Ser94 / cofactor in WT and Ala94/ cofactor binding in the complex, we present here the results based on a combination of ab initio molecular dynamics simulations[14] and analysis of the crystallographic data.

Chapter II

Methods

2.1 Structural Models

Our starting structural models are based on the X-ray crystal structures of the WT[5] and S94A[12] InhA(-Inh)-NADH adducts (PDB database entry codes 1ZID and 1ENZ) with a resolution of 2.7 Å and 2.1 Å respectively.

At the present stage, it is impossible to perform ab initio simulations on the entire proteins. Thus, the quantum calculations are limited to a portion of the NADH-binding site (Fig. 2.1), namely to complexes **I** for WT and **II** for the S94A mutant (Fig. 2.1 b and c). The models used in the present study include:

i) the β-phosphate moiety of the (Inh-)NADH group (represented as dimethylphosphate, DMP). DMP was taken as deprotonated, e.g. negatively charged, as is found in nature (physiological pH) for NADH molecule[15]. This choice is also supported for an analysis of optimal H-bond pattern inside the active site.

ii) the Ala22, Ile21 and Gly14 backbone atoms.

iii) the Ser94 (or Ala 94) residue

iv) the water molecule (WAT1) which bridges NADH β-phosphate to the enzyme pocket.
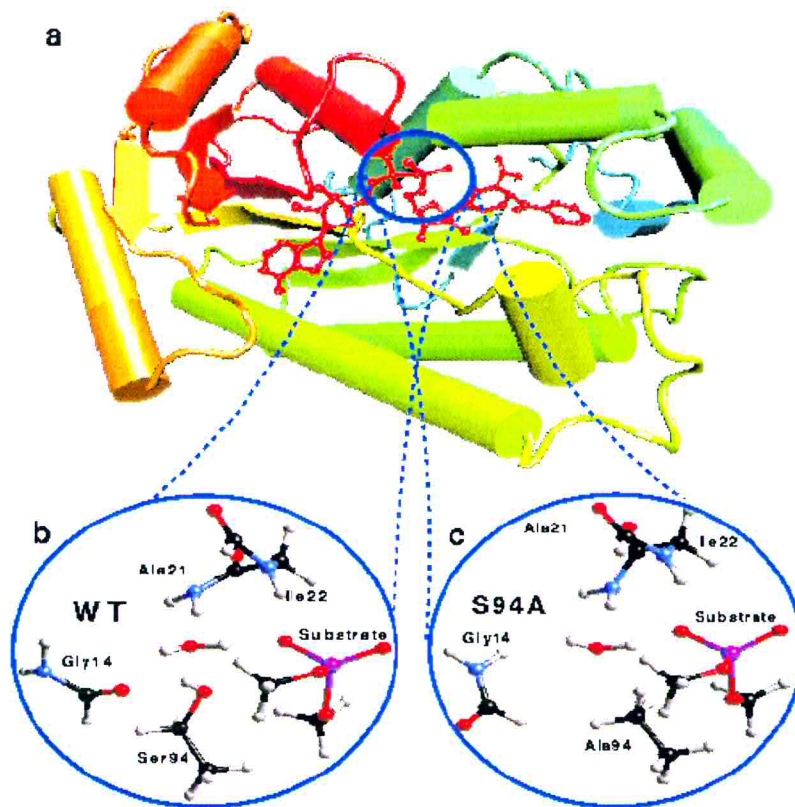
Figure 2.1: a) Cartoon representation of InhA enzyme (1ZID).Close up on the region of interest. Quantum models. b) WT (1ZID) and c) S94A (1ENZ)

These models take into account all the crucial interactions between NADH β-phosphate and the region of the binding pocket involved in the S94A point mutation. They include the following H-bond interactions: $O2$(β-phosphate)–NH (Ile21), $O2$(β-phosphate)–H2(WAT1), Ow(WAT1)–NH (Ala22), H1(WAT1)–CO (Gly14) and Ow(WAT1)–OH(Ser94) (only in WT)

Classical Molecular Dynamics (MD) simulation of the entire InhA enzyme plus the cofactor (Inh-NADH) and water molecules present in the crystallographic structure have been performed in the NPT ensemble within an explicit aqueous solution.

2.2 Quantum Calculations.

The quantum problem has been treated within a first principles Density Functional Theory (DFT) framework. Gradient-corrected exchange and correlation functionals of the Becke[16] and Lee-Yang-Parr[17] (BLYP) type were adopted. We used a plane-wave basis set up to an energy cutoff of 70 Ry. The interactions between ionic cores and valence electrons were described by Troullier-Martins[18] pseudopotentials. The complexes were treated as isolated systems[19]. This computational setup has already been proven to describe H-bonding systems with high accuracy [20;21] and it has also been extensively tested in the description of biological systems[22;23 24;25], such as phosphate binding proteins [26].

Geometry optimizations were performed using the method of direct inversion in the iterative sub-space[27] up to an energy gradient of 10^{-4} and 10^{-6} for the ions and electrons respectively.

Density functional theory based molecular dynamics were carried out for complex I using the Car-Parrinello approach[14]. 3 ps of MD were collected. A timestep of 0.121 fs (5 a.u.) and a fictitious electron mass of 500 a.u. were used.

Simulations have been performed at constant temperature achieved by coupling the system to a Nose[28]-Hoover[29] thermostat at a frequency of 500 cm^{-1}.

Following a well-established procedure[24;25], position constraints were imposed on terminal atoms of phosphate and Ala22, Ile21, Gly14 and Ser94 residues, so as to mimic the presence of the protein and substrates frames.

Calculations were carried out with the CPMD V3.0h program developed by Hutter *et. al*[30]

2.2.1 Calculated Properties

Bond ionicity indexes (BII's)[31]:

BII's provide an estimate of polarity of a chemical bond in terms of Pauling electronegativity[32]. BII's have been calculated from the centers of the maximally localized Wannier orbitals[33;33;34]. We have calculated BII's variations upon a change of chemical environment (e.g. gas phase, bulk phase, and within the protein environment).

Polarization Effects:

The rearrangement of electronic density $(\Delta\rho)$[35] on water molecule WAT1 (Fig. 1.1) upon formation of the complex has been calculated according to:

$$\Delta\rho = \rho_{(complex)} - \rho_{(complex\ without\ WAT1)} - \rho_{(WAT1)}$$

The volume integral of $\Delta\rho$ (Δq) provides a quantitative measure of polarization effects.

Binding Energies:

Contribution of the fragments have been calculated as the energy difference in the presence and in the absence of the water molecule between each one of the single molecules forming the system as follows:
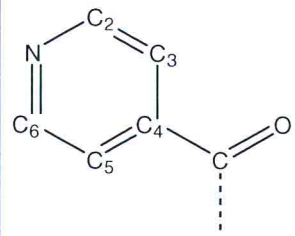
$$\Delta E1 = E_{(complex)} - E_{(fragments)} - E_{(WAT1)}$$

$$\Delta E2 = E_{(complex\ without\ WAT1)} - E_{(fragments)}$$

2.3 Classical Molecular Dynamics.

The system consisting of InhA enzyme (1ZID), Inh-NADH and crystallographic waters were immersed in a box of about 5800 water molecules. The SPC/E[36] water model was used to solvate the molecule. Calculations were made with the Gromos96 force field and Gromos96 suite of programs. Inh-NADH partial charge distribution parameters were derived by analogy with very similar chemical functional groups existent in the Gromos96 database (see Gromos96 Manual and Table 2.1).

Table 2.1 : Partial Charge distribution for the INH fragment adopted for the classical MD simulation.

Atom Name	IAC*	Charge group*	Partial Charge
C	11	0	0.38
O	1	1	-0.38
C2	16	0	0.1
C3	16	0	0.0
C4	14	0	0.0
C5	16	0	0.0
C6	16	0	0.1
N	8	1	-0.2

*IAC=Integer Atom Code (see Gromos96 manual)

Periodic boundary conditions were applied. For the treatment of non bonded interactions the twin–range cutoff method[37] was used, with cutoffs of 10 Å and 15 Å updated every 5 and 20 simulation steps respectively. Reaction field corrections for the long range

electrostatic interactions were used[38]. All bonds were constrained using the SHAKE algorithm[39] so that a time step of 2 fs was used. Constant temperature and pressure conditions were achieved though a Berendsen bath[40] with 0.2 ps relaxation time. The systems underwent energy-minimization and 0.2 ns of thermal and pressure equilibration. Finally, 1 ns MD simulations were performed at 300 K.

Chapter III

Results

3.1 Energetics

This section describes the structural and electronic properties of two geometry optimized complexes representing the binding site of *Mycobacterium tuberculosis* InhA enzyme, namely the wild type in complex **I**, and the S94A mutant complex **II**.

3.1.1 Wild-type (complex I)

Fig 3.1a shows the geometry optimized structure of model **I**, representing the wild type binding site. The structural properties of the DMP ligand and protein fragments correspond nicely either with experimental data and with those of previous high level calculations (Table 3.1). DMP molecule is found in a canonical low energy trans-gauche conformation as expected from the corresponding X-ray structural data.

A complex H-bond network is present in the active site: The O2 atom of the phosphate moiety hydrogen bonds (see Fig 3.1 for labeling) to the main chain hydrogen of Ile21 and the well ordered water molecule. Notably, this water molecule forms as many as four hydrogen bonds (namely to the hydroxyl group of Ser94, the carbonyl oxygen atom of Gly14 and the main chain hydrogen atoms of Ala22 and Ile21), bridging the ligand with the enzyme pocket.
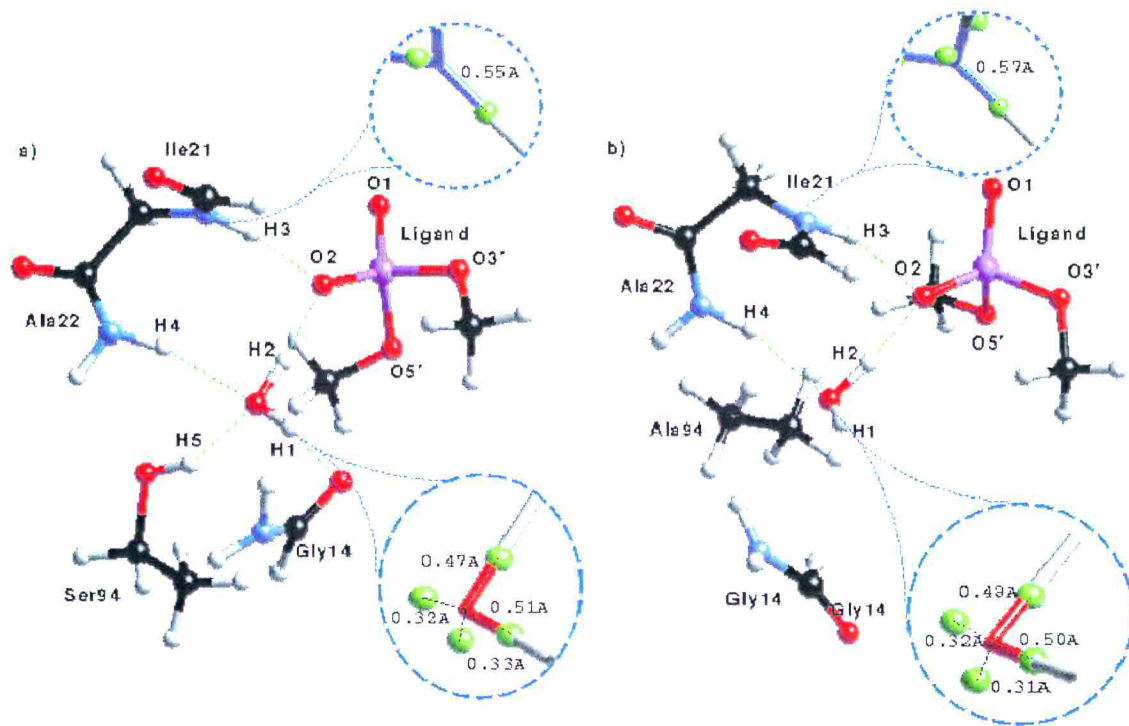
Figure 3.1: Ab initio geometrically optimized structures for a) WT (complex I) and b) S94A (complex II). H-bond pattern is shown in green dashed lines. Draws in blue circles depict the position of the centers of the maximally localized Wannier functions (green balls)

The OH bond length of the water molecule hydrogen bonding the ligand is significantly increased in comparison to the bulk water (from 0.98 Å to 1.02 Å).

Furthermore, from the displacement of the Wannier's centers we observe significant polarization effects present in this water molecule which are mainly induced by the electric field of the negatively charged phosphate group.

Table 3.1. Ab initio geometry optimized structural parameters for DMP. Comparison is made with WT[5] and S94A[12] Inh-NADH InhA crystal structures. Estimated standard deviations are given in parentheses.

	This work		X-ray (PDB entries 1ZID and 1ENZ respectively)		DMP in vacuum[31]
	WT	S94A	WT	S94A	*****
Bond lenghts [Å]					
P-O3'	1.64	1.64	1.59(0.25)	1.58(0.1)	1.68
P-O5'	1.66	1.66	1.61(0.14)	1.68(0.11)	1.68
P-O1	1.49	1.49	1.51(0.2)	1.56(0.09)	1.49
P-O2	1.53	1.53	1.47(0.17)	1.52(0.02)	1.49
Bond angles [degrees]					
O3'-P-O5'	99	99	101	102	99
O3'-P-O1	109	109	112	100	105
O3'-P-O2	109	109	101	112	105
O5'-P-O1	106	107	109	107	105
O5'-P-O2	106	108	108	107	105
O1-P-O2	120	119	122	127	125

3.1.2 Ser94Ala mutant (complex II)

In the X-ray structure of S94A InhA/Inh-NADH complex, the mutation does not lead to significant overall structural changes. The only important difference consists in the rearrangement of the carbonyl group of Gly14. Fig. 3.1b reveals a reorientation of the Gly14 backbone, as the carbonyl group facing away from the phosphate, disrupting the Gly14-WAT1 hydrogen bond present in the wild-type structure. Moreover, the loss of the Ser94 hydroxy group reduces the number of water enzyme contacts from four in complex **I** to two in complex **II** (namely to the backbone amid group of Ala22 and to the O2 in the phosphate ligand). Reducing significantly the binding energy of the ligand, since the water molecule bridges no longer the enzyme body to the phosphate moiety.

In order to analyze the physical basis of the active-site rearrangement, we have calculated the electrostatic interactions between the single fragments of the complex up to the dipolar expansion. The reason for the perturbation of the hydrogen bond network is found in the

14

electrostatic charge-dipole interactions between the phosphate and the Ser/Ala 94 and the Gly14. The major cause for the reorientation of the Gly14 is the strong charge-dipole repulsive interaction with the negatively charged phosphate. We found an energy gain of about 2 kcal/mol upon the Gly14 rearrangement.

Moreover, the torsional angles of the DMP of the geometry optimized complex **I** turn out to be slightly more bent towards the enzyme body than in complex **II**, revealing a stronger attractive interaction in the WT structure.

3.2 Chemical Bonding Analisis

The partial loss of the water hydrogen bond network has impact on the binding energy of the DMP-enzyme. Indeed, the Ile21 H-bond turns out to be less polarized in the mutant case (see Table 3.2). The H-bond distance is increased from 1.72 Å in the wild-type to 1.88 Å (see Table 3.1) in the S94A mutant and thus is expected to be significantly weaker (roughly estimated in a 30 %). This agrees with experiment, which exhibits a five-fold reduced binding affinity for the natural substrate in the S94A mutant in comparison to the wild-type[12].

Table 3.1: H-Bond distances[Å] for geometry optimized systems. Atom labeling as in Fig.3.1

	Wild Type	S94A Mutant
H1 - O (Gly14)	2.04	- not present -
H2 - O2	1.65	1.62
H3 - O2	1.72	1.88
H4 - O (water)	2.1	1.99
H5 - O (water)	2.01	- not present -

A quantitative estimate of the bond polarization is given by the shift of localized Wannier orbitals. This kind of analysis has been proved to be a very powerful tool to characterize the nature of the chemical bonds. The location of the centers of the Wanniner functions can be related with the ionicity of the bonds[31].

Table 3.2 shows the polarization effects on the water's OH (towards the O2 phosphate oxygen) on passing from gas to bulk, and from the bulk to the protein environment, confirming that the strongest H-bond interactions are found in the water-phosphate-protein complex ($BI_{OH2}(O)$ as low as -0.19). Strongly indicating that water mediated phosphate-enzyme interactions are of significant importance to the binding of the β-phosphate unit. No significant differences were found for the water in the two systems, essentially because of dominant effects are due to the proximity of the charged phosphate moiety.

3.3 Molecular Dynamics

3.3.1 Ab initio MD simulations

Even when al previously reported static calculations offer important information of the scenario we are dealing with, the key role of temperature effects has been up to here completely neglected. To take in account temperature effects on the different interacting parts of the system we have performed a 3 ps long *ab initio* MD simulation at room temperature of the wild type system.

The conformation of the β-phosphate moiety of NADH is kept *trans-gauche* as being found in the initial structure. Surprisingly, Ser94 moiety does not keep its conformation during the dynamics. Indeed, at the beginning of the dynamics, its hydroxyl points towards the water molecule and O2 β-phosphate oxygen ($\chi_1 = 171°$) and it is in H-bonding contact with

WAT1, as is found in the crystallographic structure (d(Ow-H5)=2.1 Å). However, after $\approx$ 1.4 ps, the hydroxyl group turns out facing away from the phosphate moiety (χ_1=-70°) [1], no longer bridging the water molecule. (this particular conformation will be referred hereafter as complex **Ib**). This conformation is kept over the last 1.6 ps of the dynamics (See Fig 3.2). Thus, our calculations suggest that the barrier upon rotation is lower than K_BT and that the flipped conformation is allowed and stable in the time scale investigated.
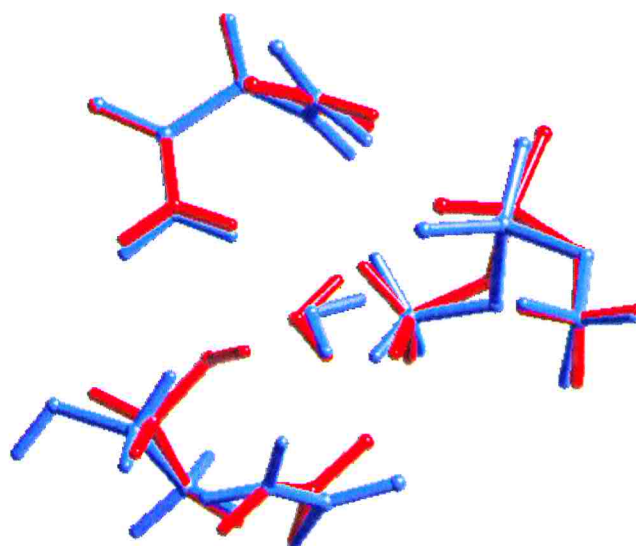
Figure 3.2: Superposition of initial (complex Ia, red) and final snapshot of quamtum MD (complex Ib, blue)

Inspection of the X-ray crystal structure[5] (1ZID) indicates that the latter conformation is sterically possible also in the presence of the protein environment. Moreover the same alternative conformation (χ_1=-84°) has been observed in a more recent X-ray crystal structure of InhA with bound NADH and mycolic acid [13] (PDB entry 1BVR) for one of the

---

[1] χ_1 value averaged over the last 1.25 ps

six molecules present in the asymmetric unit (chain E). The water mediated hydrogen bonding between Ser94 and P_N's O2 therefore no longer exists. Interestingly, a slightly different conformation for the phosphates moieties in the InhA cofactor has been also observed in this same molecule.

The loss of the H-bonding interaction has clear consequences on the dynamics of WAT1: i)WAT1 gets closer to the negatively charged phosphate group. Binding energy calculations (see Methods section) indicate that the contribution of the H-bonding term to phosphate to the total WAT1/enzyme pocket energy interaction increases from ≈ 40% to ≈ 60% on passing from **Ia** to **Ib**

ii) WAT1 displaces from its original position causes a weakening of the WAT1-Gly14 H-bond, which ultimately breaks down. The loss of the weak H-bond interaction is counterbalanced by a decrease of electrostatic interaction: Gly14's dipole reorients so as to minimize its interaction with the phosphate negative charge. A simple electrostatic model suggests that the electrostatic energy associated to Gly14 rotation is ≈ -2 kcal/mol. The only H-bond of WAT1 which is not affected from Ser94 motion is that with Ala22 backbone amide group.

3.3 Comparison between WT MD and X-ray S94A structures

In the X-ray structure of S94A InhA/Inh-NADH complex, the mutation does not lead to significant overall structural changes. The only important difference consists in the

rearrangement of the carbonyl group of Gly14, which faces away from the nucleotide (complex **II**).

WAT1 acts as an H-bonding acceptor from the Ala22 backbone amide group (d(H4-Ow=1.99 Å)) and as a H-bonding donor to phosphate's O2 (d(H3-O2= 1.88 Å)), that is *forms the same H-bond network as in MD WT final snapshot **Ib**.*
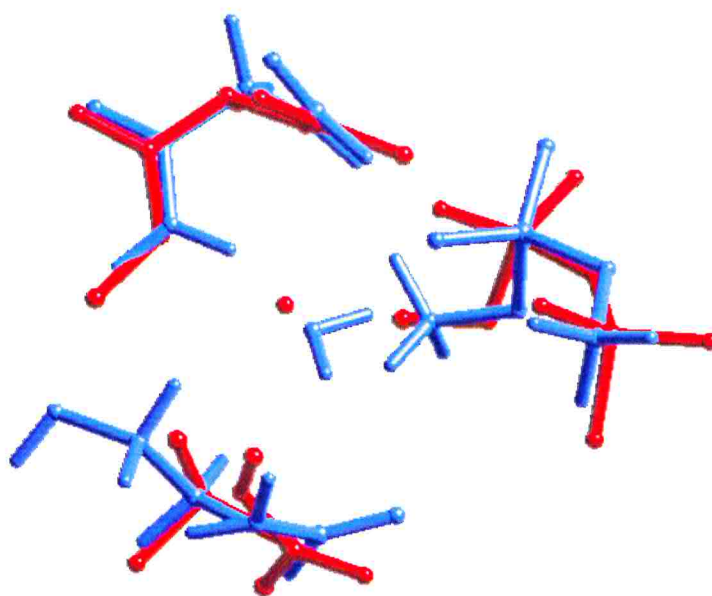
Figure 3.3: Superposition of Complex Ib (blue) and X-ray S94A (red) structures. RMS between backbone atoms=0.3

Superposition of x-ray structures of S94A mutant with complex **Ib** confirms the striking similarities between H-bond pattern and conformational properties of the two structures (rms on backbone atoms only 0.3 Å). In particular, also in the point mutant S94A, Gly14 is involved in a more favorable electrostatic interaction with the charged phosphate moiety. The electrostatic energy gain to this conformation is ≈ 2 kcal/mol, that is the same as in

MD WT. It is worthy of note that this value nicely reproduces the experimentally estimated

for S94A mutant[12].

Table 3.2. Selected ab initio MD-averaged structural parameters of. Comparison is made with WT[5] and

S94A[12] Inh-NADH InhA crystal structures. Estimated standard deviations are given in parentheses.

| Bond Lenghts [Å]				
	Complex Ia*	x-ray WT	Complex Ib*	x-ray S94A
P-O3'	1.65(3)	1.59(0.25)	1.65(3)	1.58(0.1)
P-O5'	1.66(3)	1.61(0.14)	1.67(3)	1.68(0.11)
P-O1	1.49(2)	1.51(0.2)	1.49(3)	1.56(0.09)
P-O2	1.53(3)	1.47(0.17)	1.54(3)	1.52(0.02)
Angles [Degrees]				
O3'-P-O5'	99(4)	101	99(4)	102
O3'-P-O1	109(4)	112	109(4)	100
O3'-P-O2	108(4)	101	109(4)	112
O5'-P-O1	112(4)	109	111(4)	107
O5'-P-O2	106(4)	108	106(4)	107
O1-P-O2	120(4)	122	121(4)	127
Torsional Angles [Degrees]				
C-O3'-P-O5'	147(5)	119	149(5)	156
C-O5'-P-O3'	-67(5)	-82	-67(5)	-76

*Data averaged from 0-1.25ps and 1.75-3ps respectively for complexes Ia and Ib

An analysis of the electronic structure confirms that a similarity exists in the chemical

environments of WAT1 in either the complex Ia and in the crystal structure of the point

mutant S94A :

i) the rearrangement of the electronic density of WAT1 $\Delta\rho$ upon binding to the protein is

similar (Fig. 3.4). Consistently, the charges integrated over the water molecules are

almost identical ($\Delta q=0.34$ e⁻ and 0.36 e⁻ for Ib and II, respectively)

ii) the chemical bonding is similarly affected by the protein frame in the two complexes. In

fact, the changes of OH bond ionicity indexes (BII's)[31] upon formation of the complex are

exactly the same in the two complexes. Both bonds are more polar in the enzyme relative to the gas phase. OH1 and, OH2 bonds are more polar because of they H-bond to Gly14 and β-phosphate.
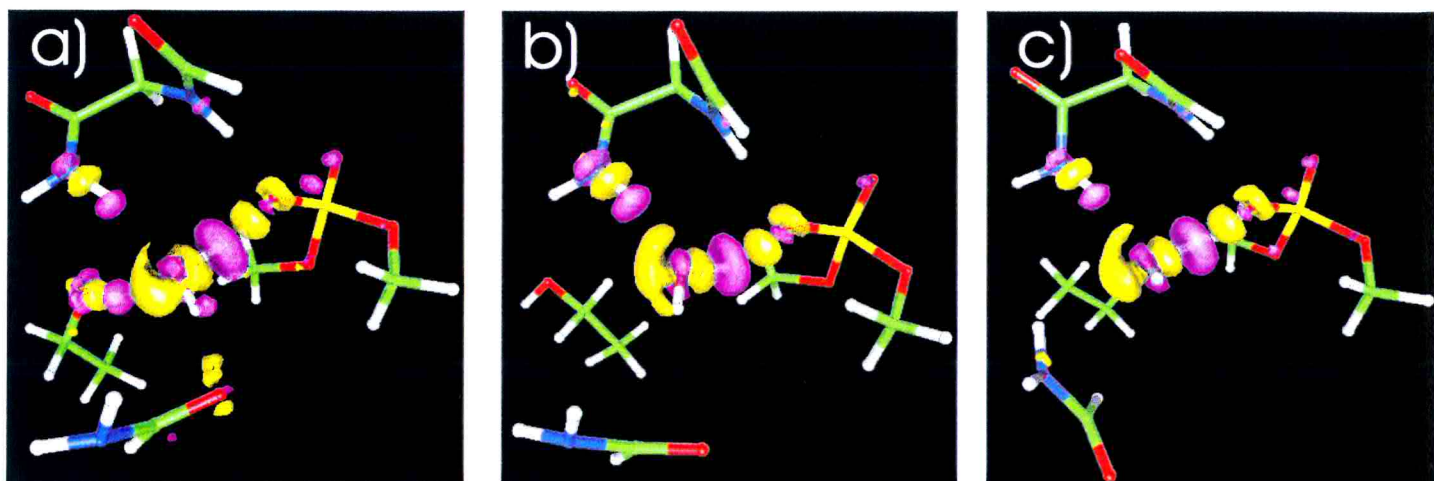
Figure 3.4: Δρ of complexes Ia (a), Ib (b), and II (c). Isosurfaces contour at 0.0035 a.u.[3] Yellow (Pink) corresponds to negative (positive) values.

We turn now our attention to the comparison between model **II** and the *X-ray crystal structure of* WT(Ia). Fig. 3.4 a and c point out the differences between the two complex already established by crystallographic studies[5;12;12;13]. As a result of a remarkably different electronic structure of the two systems, the WAT1-phosphate H-bonding interaction *is stronger* in **II** (**Ib**) than in Ia. Furthermore, the larger number of H-bonding interactions present in **Ia** with respect to **II** (**Ib**), increseases the polarization of WAT1 (Δq=0.42 e⁻) as can be seen in Table 3.3.

Table 3.3. Calculated electronic properties of complexes Ia, Ib and II.

	Complex Ia		Complex Ib		Complex II	
Δq [electrons]	0.43(1)		0.34(1)		0.36(1)	

Chemical Bonds Polarities							
	Isolated water	Bulk water	WAT1 OH1	WAT1 OH2	Ile21 amid H Comp. Ia	Ile21 amid H Comp. Ib	Ile21 amid H Comp. II
OH BII's	-0.12	-0.15	-0.15	-0.19	-0.13	-0.12	-0.11
Bond Length [Å]	0.97	0.98	.98	1.02	1.04	1.03	1.03

3.4 Classical MD Simulations

As already mentioned, and analysis of the crystallographic structure demonstrates that the rotation of the Ser94 side chain is sterically possible in the presence of the protein environment. However, it could be possible that the existence of long range interactions (e.g. dipole-(dipole)charge) not considered in the limited quantum models could stabilize the Ser94 position. In order to answer this question a Classical MD simulation have been performed on the entire enzyme bound to Inh-NADH.
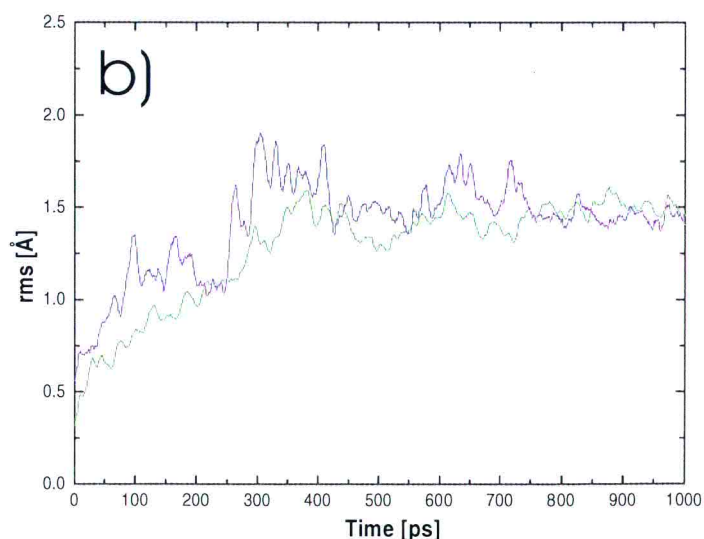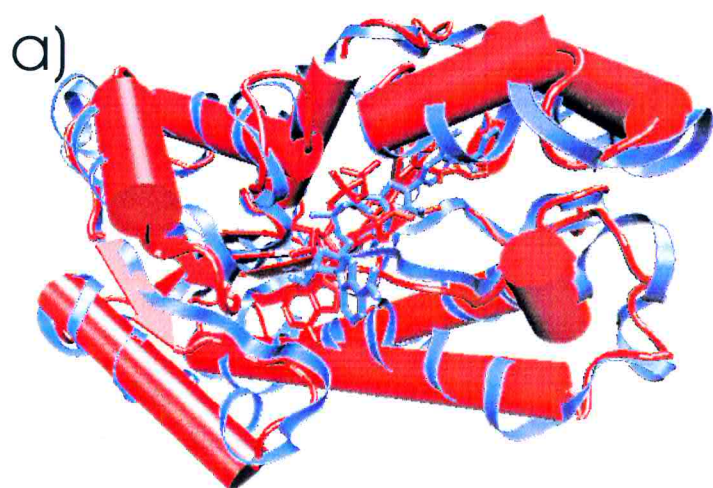

Figure 3.5: a) InhA-Inh-NADH (1ZID)crystal structure (red) and the last snapshot of the MD (blue).

b) rms of the enzyme backbone atoms (green) and Inh-NADH (blue).

To not deviate the reader's attention from the focus of our study only the MD features directly concerning the motion of Ser94 are discussed here.

Qualitatively good agreement between both classical and quantum MD features regarding water mobility and ligand conformation are obtained (data not shown). Interestingly, the rotation of the Ser94 side chain in an angle which very nicely corresponds with that one of the *ab initio* MD is also found in the classical MD simulation.

Fig 3.5 shows the time evolution after complete thermal stabilization along the Cα-Cβ torsional angle of the Ser94 for the WT enzyme bounded to Inh-NADH

Electrostatic interaction between the whole enzyme and Ser94 have been calculated using the partial charge distribution of Gromos 96 force field. This calculations give a estimation for the energy difference in the force field approach between both states (rotated and not) of ~ 2.5 kcal/mol. Which roughly corresponds with ab inito results.
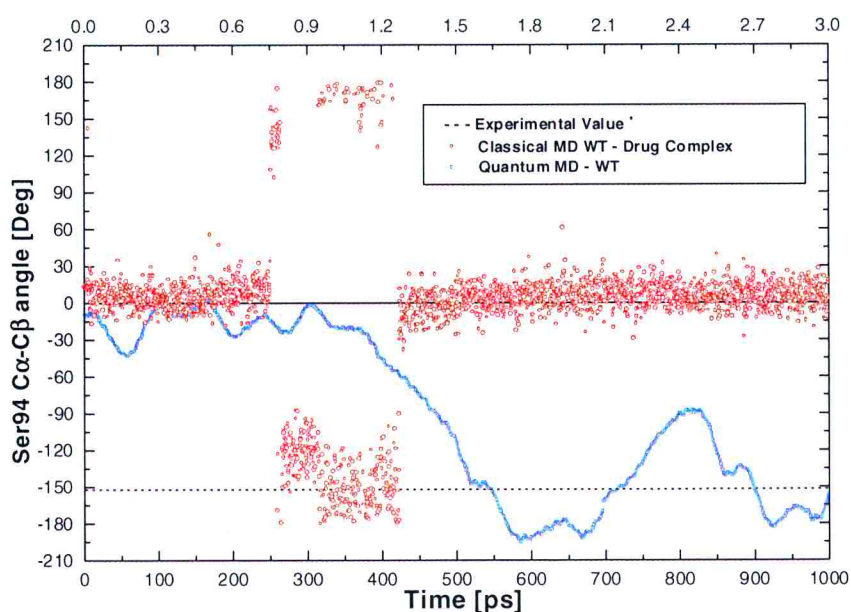

Figure 3.6: Time evolution of Cα-Cβ. Top scale: ab initio MD. Bottom scale: Classical MD. * Dashed line: corresponding dihedral angle of the crystallographic structure 1BVR (chain E)

This result clearly demonstrates not only that the rotation of the serine is allowed by the steric environment of the protein but also that it is also energetically possible.

3.4 Analysis of the Debye-Waller factors of X-ray WT

A detailed analysis of the experimentally-derived Debye-Waller (DW) thermal factors for the Ser94 side chain and the water molecule WAT1 in the crystal structure of WT (entry 1ZID of the PDB databank) revealed extremely low values. Moreover, the DW factors of the backbone atoms of Ser94 are considerably higher than those of the side chain. In addition, we have observed no continuity in the thermal factor values along the H-bonding path $O\gamma$-Ow-O2 (See Fig 3.6) as it would be expected for a stable H-bond. Controversially, the water oxygen appears to be much less mobile than the phosphate moiety and backbone atoms.

Our calculations, which instead point to a larger mobility, do not agree with the reported data. However, we argue here that these extremely low temperature factors (values of 2.0 Å^2 are repeatedly found in the deposited coordinates) might be the result of artifacts during the crystallographic refinement. Indeed, the refinement program protocol used by the authors of ref. 5 uses a minimum default value of 2.0 Å^2 as DW (see XPLOR[41] manual at the section 'Individual B-Factor Refinement'). Furthermore, the alternative conformation for Ser94 revealed by our simulations has been also observed in another InhA-NADH complex[13] (entry 1BVR of the PDB database, chain E). Therefore, we argue that our results are absolutely consistent with experimental data and that the alternative conformation for Ser94 in Inh-NADH / WT complex cannot be ruled out.
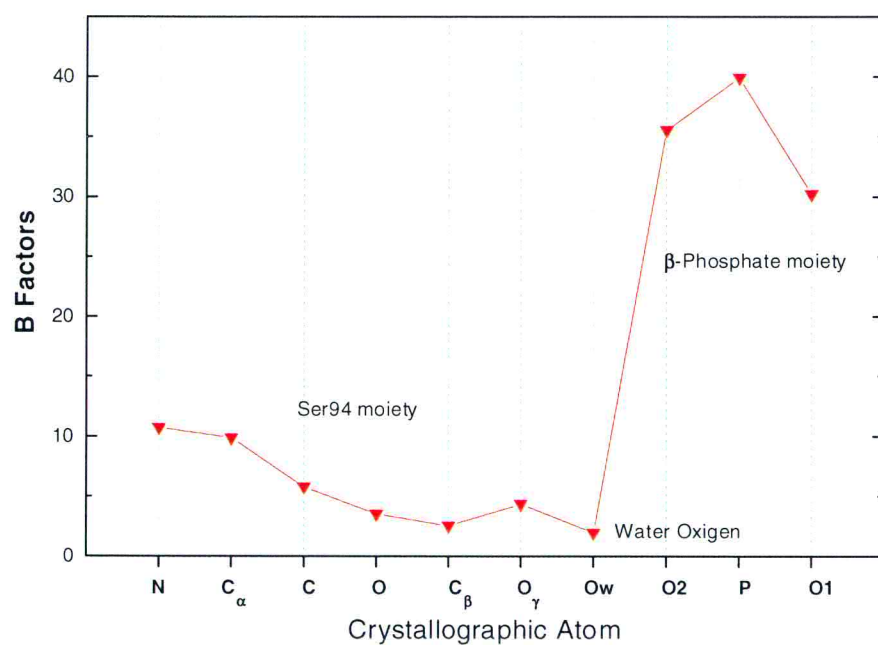
Figure 3.7: Thermal (Debye-Waller) B factors of Ser94, Crystallographic water oxygen (WAT1) and Phosphate moiety involved in the H-bond. Data from 1ZID PDB structure.

Chapter IV

DISCUSSION and CONCLUSIONS

The slightly higher affinity of WT for Inh-NADH relative to S94A has been ascribed to the presence of a weak, water-mediated interaction with the cofactor (Fig. 1.1). Here we have performed a theoretical study on a model of the InhA WT/Inh-NADH complex to characterize energetical and dynamical properties and chemical bonding of Ser94.

From the *ab initio* geometry optimizations and energetics analysis, in addition to the already reported disruption of the H-bond pattern upon the mutation, it comes out that the presence of the OH serine group in a way activates the polarization of the system through the water molecule. Causing the approaching of the negatively charged phosphate moiety and a consequent stronger enzyme-ligand binding for the wild type. While for the mutated case, in absence of the hydrogen donor (Ser94), the coordination of the system is lost. Water is more attracted by the phosphate, facilitating in this way the releasing of the ligand.

In addition, from the dynamical point of view our calculations suggest that Ser94 OH group is highly mobile and the weak, water mediated interaction between Ser94 and the cofactor interaction may be lost already in the ps timescale. Indeed, WT evolves towards the Ib model, which is strikingly similar to the X-ray crystal structure of the point mutant S94A (**II**) in terms of both geometrical parameters and electronic structure. In particular, WAT1 forms a very similar H-bond pattern.

Because of the short time-scale investigated, our calculations cannot tell whether the hydroxyl OH rotation of is a reversible or irreversible process. However, the energies and H-bond patterns of the two conformations are very close, strongly suggesting that both conformations are present at room temperature.

Because of the similarities between MD WT (Ib) and the X-ray crystal structure of the point mutant S94A (II), the affinity for Inh-NADH is expected to be only slightly larger in WT. This agrees with the fact that the measured Michaelis constants and V_{max} of WT barely differ from that of the point mutant S94A (see table 4.1). Indicating that stronger interactions play an important role in immobilizing the substrate in places nearer the region were the drug binds NADH.

Table 3. WT and S94 Kinetic parameters from Ref. 12.

Kinetic parameters for wild-type and S94A mutant InhA measured by following NADH oxidation at 340 nm with a Uvikon 93310 spectrophotometer (Kontron Instruments). All reactions were done in 30 mM Pipes buffer (pH 6.8) at 25°C. Standard reactions for the determination of the K_m of NADH contained 10 µM 2-trans-octenoyl-ACP, variable NADH (10 to 40 µM), and 7.5 nM InhA. Standard reactions for the determination of the maximum velocity and Km for 2-trans-octenoyl-ACP contained variable 2-trans-octenoyl-ACP (4 to 25 µM), 100 µM NADH, and 7.5 nM InhA.

Enzyme	K_m(µM)		Vmax
	2-trans-octenoyl-ACP	NADH	(µmol min^{-1} mg^{-1})
Wild-Type	2±1	8±0	2.2±0.4
S94A	3±1	38±2	3.1±0.6

Our calculations are not consistent with the X-ray-derived DW factors which point to an extermely low mobility of the water molecule WAT1 and of the Ser94 side chain. However

(as discussed in the Results section) these findings may arise from artifacts during the crystallographic refinement procedure.

The results derived by our ab initio MD simulations suggest that the expression of the S94T InhA point mutant and its kinetic characterization would be of great interest. In fact, the chemical properties of Thr side-chain are similar to those of Ser (both contain an alcoholic function). However, as Thr is bulkier than Ser, the energy barrier associated with the OH rotation along the C_α-C_β bond is expected to be higher than that of Ser. Hence, the affinity of S94T for Inh-NADH is expected to be larger than that of WT.

Bibliography

1. B. R. Bloom and Murray C.J.L., *Science* 257, 1055-1064 (1992).

2. W. Z. Bradford and C. L. Daley, *Infect.Dis.Clin.North Am.* 12, 157-172 (1998).

3. K. Johnsson, D. S. King, P. G. Schulz, *J.Am.Chem.Soc.* 117, 5009-5010 (1995).

4. A. Quemard et al., *J.Am.Chem.Soc.* 118, 1561-1562 (1996).

5. D. A. Rozwarski, G. A. Grant, D. H. R. Barton, W. R. Jacobs, Jr., J. C. Sacchettini, *Science* 279, 98-102 (1998).

6. H. A. Shoeb, B. U. Bowman, Jr., A. C. Ottolenghi, A. J. Merola, *Antimicrob.Agents Chemother.* 27, 399-403 (1985).

7. A. Quemard et al., *Biochemistry* 34, 8235-8241 (1995).

8. Cole S.T., *Trends.Microbiol.* 2, 411-415 (1994).

9. C. Kelley, D.Rouse, S.Morris, *Antimicrob.Agents Chemother.* **41**, 2057-2058 (1997).

10. K. Johnsson, W.Froland, P.Schultz, *J.Biol.Chem.* 272, 2834-2840 (1997).

11. J. M. Musser et al., *J.Infect.Dis.* 173, 196-202 (1996).

12. A. Dessen, A. Quemard, J. S. Blanchard, W. R. Jacobs, Jr., J. C. Sacchettini, *Science* 267, 1638-1641 (1995).

13. D. A. Rozwarski, C. Vilcheze, M. Sugantino, R. Bittman, J. C. Sacchettini, *J.Biol.Chem.* 274, 15582-15589 (1999).

14. R. Car and M. Parrinello, *Phys.Rev.Lett.* 55, 2471-2474 (1985).

15. W. Saenger, Principles of Nucleic Acid Structure, 1983).

16. A. D. Becke, *Phys.Rev.A* 38, 3098-3100 (1988).

17. C. Lee, W. Yang, R. G. Parr, *Phys.Rev.B* 37, 785-789 (1988).

18. N. Troullier and J. L. Martins, *Phys.Rev.B* 43, 1943-2006 (1991).

19. R. N. Barnett and U. Landman, *Phys.Rev.B* 48, 2081-2097 (1993).

20. P. L. Silvestrelli and M. Parrinello, *Phys.Rev.Lett.* 82, 3308-3311 (1999).

21. P. L. Silvestrelli, M. Bernasconi, M. Parrinello, *Chem.Phys.Lett.* 277, 478-482 (1997).

22. U. Roethlisberger and P. Carloni, *Int.J.Quantum Chem.* 73, 209-218 (1999).

23. U. Roethlisberger, P. Carloni, K. Doklo, M. Parrinello, *J.Biol.Inorg.Chem.* (2000).

24. S. Piana and P. Carloni, *Proteins* 39, 26-36 (2000).

25. L. De Santis and P. Carloni, *Proteins* 37, 611-618 (1999).

26. F. Alber, O. Kuonen, L. Scapozza, G. Folkers, P. Carloni, *Proteins* 31, 453-459 (1998).

27. P. Fischer and J. Almof, *J.Phys.Chem.* 96, 9768 (1992).

28. S. Nose, *J.Chem.Phys.* 81, 511 (1984).

29. W. G. Hoover, *Phys.Rev.A* 31, 1695 (1985).

30. Hutter, J., Ballone, P., Bernasconi, N., Focher, P., Fois, E., Godecker, S., Parrinello, M., and Tuckerman, M. CPMD. MPI fur Festkorperforschung and IBM Zurich Research Laboratory(3.0h). 1996.

31. F. Alber, G. Folkers, P. Carloni, *J.Phys.Chem.B* 103, 6121-6126 (1999).

32. W. J. Hehre, L. Radom, P. v. R. Schleyer, J. Pople, Ab Initio Molecular Orbital Theory (Wiley, New York, 1986), p. 140.

33. N. Marzari and D. Vanderbilt, *Phys.Rev.B* 56, 12847-12865 (1997).

34. P. L. Silvestrelli, N. Marzari, D. Vanderbilt, M. Parrinello, *Solid State Commun* 107, 7 (1998).

35. Y. Gu and S. Scheiner, *J.Am.Chem.Soc.* 121, 9411 (1999).

36. H. J. C. Berendsen, J. R. Grigera, T. P. Straatsma, *J.Phys.Chem.* 91, 6269-6271 (1987).

37. H. J. C. Berendsen, in *Molecular Dynamics and Protein Structure*, J. ed. Hermans, Ed. (Polycrystal Book Service, 1985).

38. I. G. Tironi, R. Sperb, W. F. van Gunsteren, *J.Chem.Phys.* 102, 5451-5459 (1995).

39. J.-P. Ryckaert, G. Ciccotti, H. J. C. Berendsen, *J.Comput.Phys.* 23, 327 (1977).

40. H. J. C. Berendsen, J. P. M. Postma, W. F. van Gunsteren, A. DiNola, J. R. Haak, *J.Chem.Phys.* 81, 3684 (1984).

41. Brunger, A. T. X-PLOR, A System for X-Ray Crystallography and NMR. (3.1). 1992. New Haven, CT, Yale Univ. Press.